



# Routes for realizing high-performing Si solar cells by using periodic structures



Pankaj Yadav<sup>a</sup>, Malkeshkumar Patel<sup>a</sup>, Hyunyub Kim<sup>b</sup>, Yunae Cho<sup>c</sup>, Hyunki Kim<sup>a</sup>, Joondong Kim<sup>a,\*</sup>, Junsin Yi<sup>b,\*</sup>, Dong-Wook Kim<sup>c,\*</sup>

<sup>a</sup> Photoelectric and Energy Device Application Lab (PEDAL) and Department of Electrical Engineering, Incheon National University, Incheon, 406772, South Korea

<sup>b</sup> College of Information and Communication Engineering, Sungkyunkwan University, Suwon 440746, South Korea

<sup>c</sup> Department of Physics, Ewha Womans University, Seoul 120750, South Korea

## ARTICLE INFO

### Article history:

Received 12 December 2016

Received in revised form 10 May 2017

Accepted 10 May 2017

Available online 25 May 2017

### Keywords:

Si solar cells

Periodic structures

Light-active

Si pillars

## ABSTRACT

Theoretical suggestion indicated the substantial improvement of solar cells by using periodic structures. Yet, the promise has not been practically realized due to the lack of electrical analyses of periodical light-absorbing structure. Here, we report the record high-efficiency of 16.9% for periodically patterned silicon (Si) solar cells. Periodic Si micro-pillars were fabricated for large-scale solar cells. The Si pillars with a height of about 5  $\mu\text{m}$  provided significantly enlarged light-active surface, which improved the photo-generated carrier collection efficiency. From optical aspects, the pillar structures reduced light reflection and hence effectively drove more photons into the absorber layer. Additionally, the enhanced pillar-structured Si surface definitely contributed to reduce an electrical resistance of a solar cell. We demonstrated that the surficial enhanced Si design could be a promising approach for high-efficient solar cell applications. We may suggest a route for the optimum electrical designs of periodic structured solar cells.

© 2017 Elsevier Ltd. All rights reserved.

## 1. Introduction

Silicon (Si) is the earth abundant and well-established for the various semiconductor technologies. Especially for the photovoltaic cells, the crystalline Si widely dominates the solar cell industries. However, the cost burden of crystalline Si solar cell is remained to satisfy the cost parity with fossil fuels, which leads the developing thin-film types solar cells onto inexpensive or reusable [1,2].

The structuring of semiconductors on the nano- and micro-scale is a promising approach for the fabrication of scalable and efficient devices for the production of electricity and fuels from sunlight [3–6]. Moreover, by engineering the device geometry, the enhanced light absorption and smaller volumes of cheaper Si can be used to improve the performance of solar cells [7–14]. One such proposed approach employs micro-structured Si for the fabrication of high performance and low cost solar cells because of their

various structural advantages and the potentiality of large area-scalable fabrication. In contrast to a traditional geometry that is characterized by planar light absorbers and planar electrical junctions, micro-pillar based architectures orthogonalize the directions of light absorption and carrier collection. Such a structure provides both a long optical path length for efficient light absorption and a short distance for minority-carrier collection, therefore allowing the incorporation of defective materials with short minority-carrier diffusion lengths into devices that can produce high energy-conversion efficiencies [1,2].

Despite of its various advantages and continuous progress in the last few years [15–19], the potential of these solar cells is overshadowed by its lower efficiency and scale capability of the fabrication process as compared to the commercially available planar Si solar cells [20,21]. There are still some key aspects to be considered and design challenges to be addressed in order to exploit the advantages of micro-pillar based Si solar cells. The relatively lower efficiency of micro-structured Si solar cells are associated with the following reasons: (1) difficulty to establish a quasi-neutral region (QNR) and space charge region (SCR) in its tiny geometry [22,23], (2) surface defects generated by the direct etching of semiconductor, which may cause a lower carrier

\* Corresponding authors.

E-mail addresses: [joonkim@incheon.ac.kr](mailto:joonkim@incheon.ac.kr) (J. Kim), [yi@skku.ac.kr](mailto:yi@skku.ac.kr) (J. Yi), [dwkim@ewha.ac.kr](mailto:dwkim@ewha.ac.kr) (D.-W. Kim).

collection efficiency and degradation of the cell performance [24–27] and, (3) discrepancies between the optical and defect induced recombination losses.

Keeping in view the above-mentioned shortfalls, we have undertaken a detailed study on the fabrication of micro-structured Si solar cell of a large area. In the promising design scheme, we have fabricated micro-structures (i.e. micro-pillars) on planar semiconductor by employing dry etching method. The fabricated structure shows an overlapping of optical benefit on an electrical surface defects arising due to an increased surface area. For a micro-structured Si solar cell design to achieve the maximum

efficiency, appropriate choice of the pillar size is critical. The optimal size is of the order of the minority carrier diffusion length. In this paper we report on (1) fabrication of periodic micro-structured, large scale solar cells, (2) minimization of reflection from the incident wavelength, (3) electric analytical analysis of  $p$ - $n$  junction, and (4) light induced electric field profiles along the micro-structured patterns. We demonstrate the fabrication of high quality micro-structured Si solar cell with a power conversion efficiency of 16.90%, which is the highest among those reported from micro-structured or nano-structured Si solar cells till date [1,2,7,10]. The increased efficiency is mainly derived from the

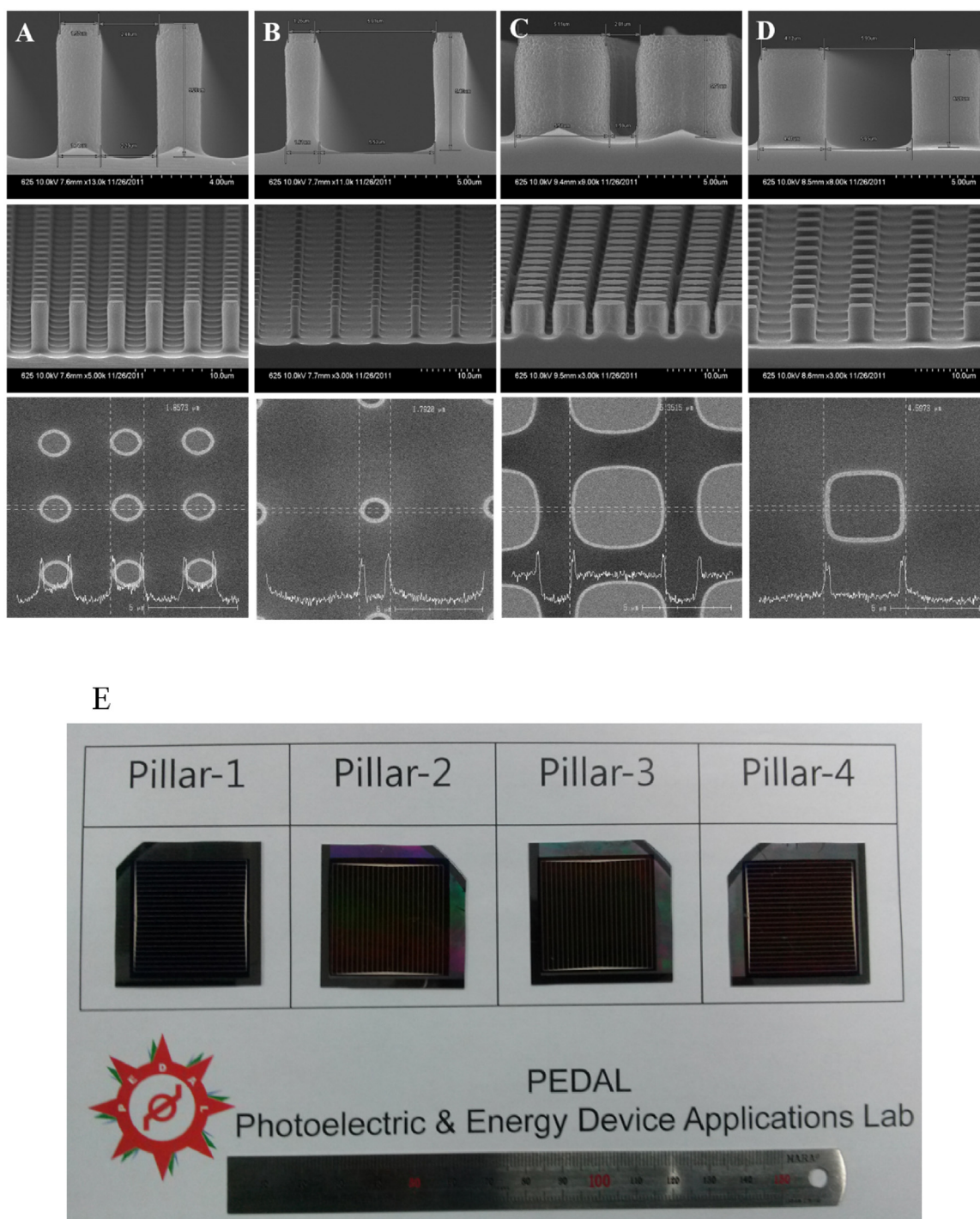


**Fig. 1.** Pillar structures of (A) pillar-1, (B) pillar-2, (C) pillar-3, (D) pillar-4. The first and second rows are for cross-sectional views; the third row is for top views and (E) Photos of fabricated solar cells.

enhancement of photocurrent and voltage through interfacial engineering of the solar cell. These results show that the micro-structured Si solar cell outperforms its planar counterpart by a low-cost, high throughput and large area-scalable fabrication process which is one of the prerequisite for these devices to be technologically viable.

## 2. Experimental procedures

Czochralski grown 500  $\mu\text{m}$  thick *p*-type (100) Si wafers having a resistivity of 1–10  $\Omega$  were used as a starting material to fabricate periodic micro-structures on a large scale for solar cell applications. In order to form the microscale Si pillar structures, the conventional photolithography processes were applied. The designed Si pillar diameters were defined as size of photoresist (PR) entities, which serve as an etching mask to protect the Si below them. Meanwhile, the exposed Si parts were etched away. During the reactive ion etching process, an initial flow of  $\text{C}_4\text{F}_8$  gas formed a polymer coating layer. After then,  $\text{SF}_6$ -plasma was employed for several loops for 10 min to etch the residual polymer layer and the exposed Si parts without the PR masks. For the formation of a *p-n* junction, *n*-type doping was done using phosphorous oxy-chloride ( $\text{POCl}_3$ ) source. After the formation of *n*-type layer, a buffered hydrofluoric acid (5% HF) solution was used to remove the phosphosilicate glass (PSG).

A thin 80 nm  $\text{SiNx}$  layer, which actively acts as an antireflection coating and passivating layer, was formed over *n*-type layer. The size of the samples was  $3.2 \times 3.2 \text{ cm}^2$  which is among one of the most efficient micro-structured solar cell with this area. The metal contacts were formed by screen printing the silver (Ag) and aluminium (Al) paste at front and back contacts, respectively, before co-firing. Planar cells with the same area but without any micro-structures were used to produce a planar junction device for the performance comparison.

The front surface reflectance profiles from the prepared devices were characterized using a diffused reflectance integrated sphere attached with UV-vis spectrophotometer (UV-2600, Shimadzu Corporation); by the reflectance spectra in the range 320–1150 nm. I–V characteristics of the prepared devices were measured using the source measure unit (2440, Keithley) for the dark and light conditions at room temperature. Solar cell performances were measured using a simulator system (McScience-K3000, Korea). This light source was calibrated using a photovoltaic power meter (McScience-K101) for one sun ( $100 \text{ mW/cm}^2$ ) illumination. Complementarily, light intensity was verified using a power meter (KUSAM-MECO, KMSPM-11). Carrier collection efficiencies of solar cells were measured using a quantum efficiency measurement system (McScience-K3100, Korea). Coupled monochromatic (Oriel Cornerstone 130 1/8 m Monochromator), source measurement unit (2440, Keithley) and lock in amplifier (K102, McScience) were applied. Mott-Schottky analyses (C-V characteristics) and impedance spectra of the abrupt *n/p* devices were obtained by using the Potentiostat/Galvanostat (ZIVE SP1, WonA Tech, Korea). The Potentiostat/Galvanostat was calibrated with a standard static and dynamic circuit before the impedance and Mott-Schottky measurement. The MS measurements were performed at 20 kHz of frequency.

Light behaviours by the micro pillar structure for the light propagation of incident light behaviors through the pillar geometry were studied using the finite-difference time-domain (FDTD) method. Maxwell's equations were numerically solved using the FDTD simulations (Lumerical FDTD Solutions). The devices were modeled with unit cells and the proper boundary conditions. The light-induced electric field ( $E_{\text{light}}$ ) intensity distributions and reflectance spectra were obtained under illumination of linearly polarized light [8,9,28].

## 3. Results and discussion

A field emission scanning electron microscope (FESEM) was used to observe the surface morphology of the micro-structured Si solar cell. Fig. 1 shows the FESEM images of the fabricated micro-structures and resultant formed geometry is summarized in Table 1. Each micro-pillar structure had a different diameter and a period at a fixed depth of about 5  $\mu\text{m}$ . The coupled geometry is made as pillar-1 and pillar-2 which has a diameter of 2  $\mu\text{m}$  with different periods of length between the pillars. The other coupled geometry is paired as pillar-3 and pillar-4 which has a diameter of 5  $\mu\text{m}$  and different periods of length. This structure modulation is the influential parameter for the enhanced interfacial optoelectronic properties between different structures [28–30]. For the micro-structured solar cell design to achieve a maximum potential efficiency, appropriate choice of the pillar size is critical.

The photoresponse of a solar cell is strongly influenced by an incident light management. Fig. 2 shows the structure dependent reflection tendencies. An average reflection value in the wavelength range of 300–1100 nm for planar Si is  $\sim 10\%$  while the average reflectance values for pillar 1, 2, 3 and 4 geometries are 8.15, 7.50, 6.00 and 8.01%, respectively. A significant reduction in the reflection values is observed for pillar-2 and 3 geometries. To quantify, the reflectance profiles are analyzed by the area under the curve method (Fig. S1). A significant reflection reduction was found from the pillar-3 to have about 50% reduced reflection.

In order to investigate the photovoltaic performance of the fabricated device, the current-voltage (J-V) characteristics under irradiation of 1 sun intensity (AM 1.5G at  $100 \text{ mW/cm}^2$ ) was done and is shown in Fig. 3A with its key photovoltaic parameters listed in Table 2. A clear trend of enhancement in device performance with the change in filling ratio, FR (%) is observed for the micro-structured devices. The filling ratio is defined as the center-to-center distance between the pillars with respect to their radius. All micro-structured solar cells, irrespective of the pillar size, showed a higher short circuit current and open circuit voltage as compared to the planar devices. Starting from the lowest FR sample (i.e. pillar-2), current density ( $J_{\text{SC}}$ ), open circuit voltage ( $V_{\text{OC}}$ ) and Fill factor ( $FF$ ) of 34.18  $\text{mA/cm}^2$ , 0.605 V and 75.46%, respectively are observed. With an increase in FR to approximately 19.6% which is obtained by employing two different pillar configurations, the values of  $J_{\text{SC}}$ ,  $V_{\text{OC}}$  and  $FF$  increases to approximately 36.47  $\text{mA/cm}^2$ , 0.60 V and 76.23%, respectively. With a further increase in FR a decrease in the values of  $J_{\text{SC}}$ ,  $V_{\text{OC}}$  and  $FF$  is observed. In conclusion, the key photovoltaic parameters i.e.  $J_{\text{SC}}$ ,  $V_{\text{OC}}$  and  $FF$  for solar cell with FR approximately 19% are remarkably greater than those from the planar and other pillar Si solar cells. The highest  $J_{\text{SC}}$  and  $V_{\text{OC}}$  for 19% FR solar cells (i.e. pillar-1) can be ascribed to the higher light harvesting and better interfacial electric field properties.

The most efficient solar cell based on pillar configuration of width 2  $\mu\text{m}$  with a period of 4  $\mu\text{m}$  exhibit a  $J_{\text{SC}}$  of 36.47  $\text{mA/cm}^2$ ,  $V_{\text{OC}}$  of 0.608 V,  $FF$  of 76.23% and power conversion efficiency ( $\eta$ ) of 16.9% which is the best reported periodically textured solar

**Table 1**  
Design parameters and the resultant formed geometry.

Parameters		Pillar-1	Pillar-2	Pillar-3	Pillar-4
Width	Design	2 $\mu\text{m}$	2 $\mu\text{m}$	5 $\mu\text{m}$	5 $\mu\text{m}$
	Fabricated device	1.58 $\mu\text{m}$	1.26 $\mu\text{m}$	5.11 $\mu\text{m}$	4.12 $\mu\text{m}$
Period	Design	4 $\mu\text{m}$	7 $\mu\text{m}$	7 $\mu\text{m}$	10 $\mu\text{m}$
	Fabricated device	4.03 $\mu\text{m}$	7.13 $\mu\text{m}$	7.1 $\mu\text{m}$	9.97 $\mu\text{m}$
Depth	Design	5 $\mu\text{m}$	5 $\mu\text{m}$	5 $\mu\text{m}$	5 $\mu\text{m}$
	Fabricated device	5.2 $\mu\text{m}$	5.43 $\mu\text{m}$	5.71 $\mu\text{m}$	6.2 $\mu\text{m}$

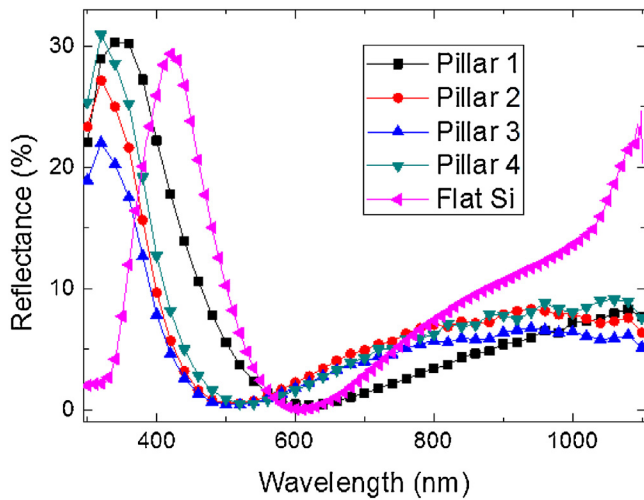


Fig. 2. Reflectance Spectra for all the micro-structured devices.

cell till date [1,2,7,10]. Hence our work also sets here a new milestone for the periodic micro-scale patterned Si solar cell.

To elucidate any ambiguity in the variation of interfacial phenomena and light harvesting properties along with its contribution to  $V_{OC}$  and  $J_{SC}$ , we studied the light and pillar geometry-induced electric field and internal quantum efficiency (IQE), respectively. Fig. 3B shows the IQE spectra for all the solar cells. The photo-generated current in a solar cell is directly influenced by the collection probability of photo-generated charge carriers as a function of effective utilization of the incident light inside the absorber layer [31]. Comparison of the IQE spectra of the micro-structured Si solar cells with the planar device indicates that the micro-structured devices clearly outperform the planar counterpart by compensating the short minority carrier lifetime of the base material.

At a shorter wavelength i.e. at 400 nm, the optimum FR 19% (i.e. pillar-1) has showed an enhanced value of IQE than that of planar Si solar cell which is due to the distinctive result of higher surface enhancement. The surface enhancement corresponding to FR 19% has been calculated. The micro-pillars are periodically arrayed with a period of about  $4 \mu\text{m}$  on the entire substrate. A single nano-pillar has a width and surficial length of  $2 \mu\text{m}$  and  $5 \mu\text{m}$ , respectively. By considering a planar surface area of 100% as a reference, the nano-pillar structure has a surface of 128% for a single unit cell, which is 28% higher than that of planar structure and approximately equal to our previous study on the nanocone based solar cells [28–30]. The current value is directly proportional to the surface area enhancement. The  $5 \mu\text{m}$  height pillar solar cells provide much higher current density values compared to those of  $2 \mu\text{m}$  height pillar solar cells [7] or hole solar cells [8]. The wavelength corresponding to 650 nm i.e. red region and 1100 nm is the most important wavelength for a Si absorber and from the bulk recombination point of view [31]. At the wavelength of 600 nm, a higher value of IQE i.e. 95% for FR 19% than that of 75% for a planar Si indicate distinctive results of optical benefit for a micro-structured Si solar cell. On the other hand, at a longer wavelength of 1100 nm a substantial IQE enhancement for FR 19% from the planar cell indicates a relieved burden of recombination loss in the micro-scale device. Therefore it can be concluded from the present and previous studies on micro-structured devices that the optical enhancement in the solar cell may stem from the surface area enhancement. However it is well reported in literature that surface patterning process almost always accompanies with surface defects that leads to the deterioration of photo-generated charge carriers by recombination [25–27]. In our results, an increased IQE for nano-structure devices throughout the entire wavelength range shows that the optical benefit surpasses the surface recombination electrical losses [28,29].

The real space electromagnetic (EM) field distribution in pillars and planar Si were investigated using finite difference time domain (FDTD) simulations [8]. Fig. 4 shows the electric field intensity

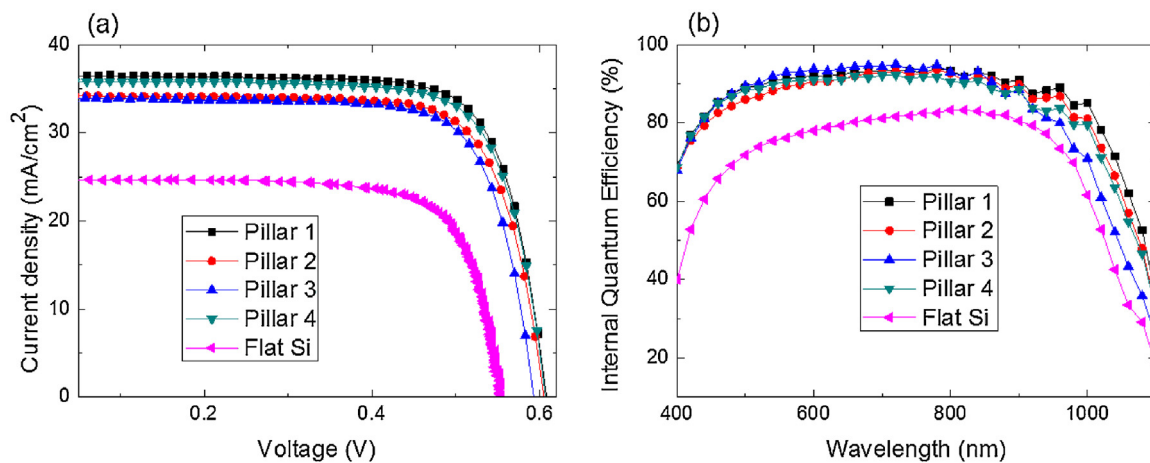


Fig. 3. (A) Light J–V characteristics under AM1.5G illumination condition for all the samples, (B) Internal quantum efficiency spectra for all the fabricated devices.

Table 2  
Performance indicating parameters of the fabricated devices.

	$V_{OC}$ (V)	$J_{SC}$ ( $\text{mAcm}^{-2}$ )	FF (%)	$\eta$ (%)	$R_S$ ( $\Omega$ )	$R_{SH}$ ( $\Omega$ )	Calculated $J_{SC}$ ( $\text{mAcm}^{-2}$ )	Filling Ratio (%)
Pillar-1	0.608	36.47	76.23	16.90	0.149	111.16	38.33	19.6
Pillar-2	0.605	34.18	75.46	15.60	0.165	169.90	37.17	6.4
Pillar-3	0.593	33.97	75.44	15.19	0.157	48.30	37.28	40.1
Pillar-4	0.607	35.84	75.97	16.53	0.149	109.89	37.01	19.6
Planar Si	0.554	24.65	74.7	10.2	0.174	652.62	27.7	–

distribution of pillar and planar solar cells under illumination of linearly polarized plane waves. With increase in depth from the surface, the EM field intensity of the incident light in a flat sample exponentially decreases. The penetration depth of light in a crystalline Si wafer is 2.4 and 145.4  $\mu\text{m}$  at  $\lambda = 600$  and 1000 nm, respectively. Thus the flat Si structure is less effective to absorb the incident light showing the relatively uniform distribution of the electric field intensity, as shown in Fig. 4. In contrast, the intensity distribution in the pillar cell is significantly distinct from that in the flat cell. Strongly concentrated light appears near the centre of the pillars at  $\lambda = 600$  and 1000 nm. Such field pattern can be attributed to guided mode excitation in the Si micro-pillars [8]. The electric field intensity is proportional to the photon flux, and hence the larger field leads to the higher density of photo-generated carriers. As a result, the amount of photo-carriers near the top surface of the micro-pillar cell is much more than that of the flat cell. The carriers at the top region of the cell are supposed to have high collection probability, since the built-in electric field is present in SCR near the surface. In addition to this, the small pillars have a more intense field distribution at center and edges as compared to the larger pillars. The obtained intense electric field distribution and optical enhancement in the pillar structure as compared to the planar Si signifies that we have conceived a micro-structured device to take the advantage over both the optical and electrical characteristics.

In order to investigate the quality of  $p$ - $n$  junction, the J-V characteristic under dark is performed and shown in Fig. 5A. The J-V characteristic of a solar cell under dark in forward bias (FB) signifies that the recombination current is due to the trap and surface states [32–34]. Three different regions are identified in the probed bias range. In the low FB region, the net  $J$  is approximated as  $V/R_{SH}$  and characterized by a shunt leakage current  $J_{SH}$ . By comparing the device performance of all the fabricated cells it is observed that the planar structure solar cell exhibits a lower value

of  $J_{SH}$  which signifies a higher shunt path or lower shunt leakage current. The higher leakage current in micro-structured devices may be arises from the enhanced interfacial surface area. As a consequence of higher leakage current, degradation in the solar cells  $V_{OC}$  can be estimated. However, in our samples no such degradation was observed and the results are in consistent with our previous reports on nanocone solar cells [28,29].

The empirical relation between leakage current and  $V_{OC}$  of a solar cell is given by  $V_{OC} = kT/q \ln(I/J_{RS})$ , where  $J$  is the net light current and  $J_{RS}$  is a defect induced current. However, in comparison with the planar structure, an increase in  $J_{RS}$  for micro-structured solar cell was sufficiently relieved by significant increase in  $J$ . In the marked region II, the logarithmic change in  $J$  is almost parallel with reference to the planar structure while in region III the logarithmic change in  $J$  of micro-structured solar cell tends to be lower than the current in planar structure. In this probed bias region, the recombination current is mainly dominated by quasi-neutral region (QNR) and the resistive losses are due to the series resistance ( $R_S$ ). An additional significance of the conclusion drawn from region III can be obtained by quantifying the series resistance of the solar cell from the reciprocal value of the linear slope of J-V curve near open circuit voltage. A lower value of  $R_S$  ( $4 \Omega \text{ cm}^2$ ) for pillar-1 solar cell as compared to the planar structure ( $R_S$  of  $9 \Omega \text{ cm}^2$ ) has a striking impact upon the device FF [35,36].

To further quantify the role of enhanced surface area on the diode ideality factor, the effective ideality factor ( $m_{eff}$ ) of planar and pillar-1 solar cell as a function of applied bias are shown in Fig. 5B. The  $m_{eff}$  as a function of applied bias was calculated using the charge coupled defect model discussed by Breitenstein et al. [34]. By employing the diode equation i.e.  $J_0 \exp(qV/m_{eff}k_B T)$ , where  $J_0$  represents the saturation current density,  $m_{eff}$  represents effective ideality factor,  $q$ ,  $k_B$  and  $T$  represents the electronic charge,

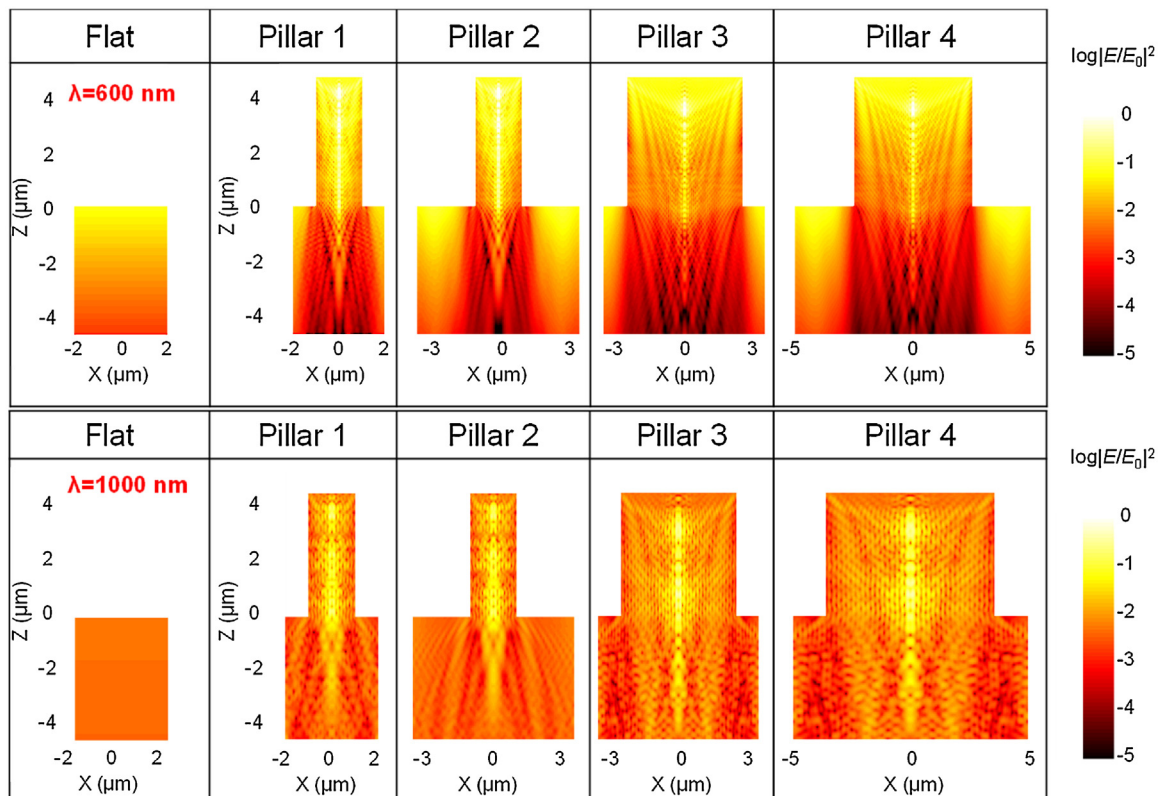


Fig. 4. Light induced electric field intensity distribution under linearly polarized light for all the fabricated devices.

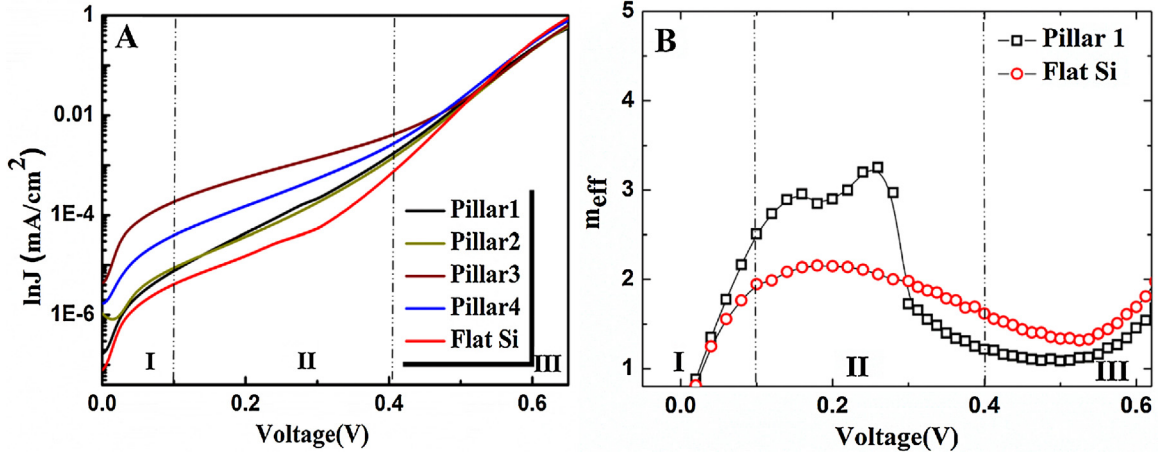


Fig. 5. Dark J-V characteristics of the fabricated devices, (B) variation of effective diode ideality factor as a function of applied bias for the most efficient micro-structured device and the planar Si solar cell.

Boltzmann’s constant and cell temperature respectively. Under the condition where  $\exp(qV/m_{eff}k_B T) > 1$   $m_{eff} = \left[ \frac{k_B T}{q} \ln \left( \frac{d \ln J}{d V} \right) \right]^{-1}$  the value of  $m_{eff}$  can be approximated as

The marked line in Fig. 5B indicates the different bias region discussed in the previous section. In a wide region II, the value of  $m_{eff}$  for both the solar cells is over two. There are various models adapted in literature to explain the value of  $m_{eff} > 2$  [37,38]. The  $m_{eff}$  in a range of  $3.2 \geq m_{eff} \geq 1.2$  are well explained according to the coupled defect model [34]. As we are mainly concerned with an increased  $m_{eff}$  value corresponding to an enhanced surface area, it is shown that with a 27% increase in surface area (pillar-1) the value of  $m_{eff}$  increases by 25% which is sufficiently relieved by 47% increase in the photocurrent. However, for the value of  $m_{eff}$  between 3.2 to 1.2 the coupled defects are only activated when at least one type of the two participating recombination trap is shallow which is typically lying at  $>10k_B T$  from the intrinsic Fermi level,  $E_i$  [39].

The particular recombination is strongly dependent upon the strength of electric field at SCR. The enhanced electric field in the SCR of micro-structured solar cell (discussed in Fig. 4) further suppresses the influence of defect induced recombination. On the other hand, in Region III an approximately equal value of  $m_{eff}$  for both the solar cells signifies that the probed bias region is mainly dominated by series resistance which further supports the fact that in Fig. 5A the change in the slope of  $\log J$  vs. applied bias is due to  $R_s$  (Fig. 6).

Impedance spectroscopy (IS) technique was employed here to reveal the mechanism for higher  $V_{OC}$  in a micro-structured solar cell as compared to the planar Si solar cell. IS technique depicts the dynamic information about the charge transport, recombination and accumulation in the devices [35,40,41]. However, its interpretation is not trivial but once an appropriate model with proper limiting conditions is developed this technique allows to separate characteristic features of different interfaces and layers in the device [40,41].

IS characterization was conducted under the dark condition in order to avoid any influence of enhanced light capturing effect in micro-structured devices. For the performance comparison, the best efficient micro-structured pillar (i.e. pillar-1) solar cell was compared with the planar device. The corresponding IS spectra for both the solar cells under dark condition is given in the electronic Supplementary information (ESI†, Figs. S2, S3). The recombination resistance ( $R_{rec}$ ), which reflects the device recombination or

diffusion mechanism due to the change in the carrier density was extracted from the low frequency arc of the IS spectra. The details of the IS spectra and various frequency responses of different interfaces of Si solar cell were discussed in detail in our previous articles [20,21,36].

From the variation of  $R_{rec}$  as a function of applied bias, it is found that the value of  $R_{rec}$  is lower for planar structure than that of micro-structured devices. It has been seen for a bias corresponding to the knee voltage the value of  $R_{rec}$  is lower by 50 mV than that for micro-structured device. This indicates that for a given bias condition, the micro-structured device upshift the conduction band edge by the level of 50 mV relative to the planar solar cell and results in the enhancement of Fermi level splitting. It is to be noted here that with respect to the conduction band upshift, the valence band Fermi level shift is insignificant for both the solar cells because the induction of extra holes causes an insignificant change in the majority charge carriers [36]. The higher upshift of the conduction band edge in micro-structured solar cell is in good agreement with the enhancement of  $V_{OC}$ . The enhanced  $V_{OC}$  and upward shift of conduction band edge in micro-structured devices can be explained by the SCR dominated recombination mechanism through higher bias as compared to the QNR dominated recombination in the planar device. The consequences of the dominance of QNR recombination over the SCR and its influence on

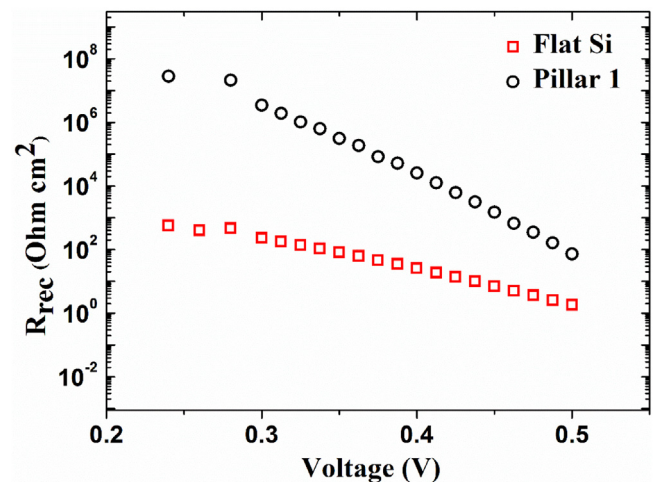


Fig. 6. Variation of recombination resistance extracted from the IS spectra for the most efficient micro-structured device and the planar Si solar cell.

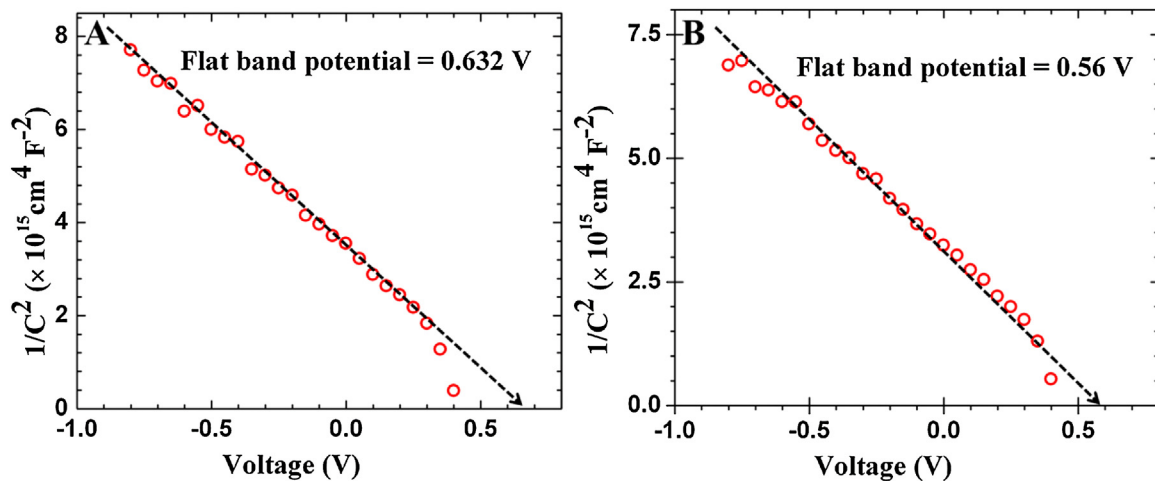


Fig. 7. Mott Schottky plot for (A) most efficient micro-structured device, i.e. pillar-1 solar cell and (B) the planar Si solar cell.

solar cells  $\eta$ ,  $FF$  and  $V_{OC}$  were discussed in detail in our previous reports [36,42]. As a result a strong domination of SCR recombination including an upward shift of conduction band edge in a resultant device enhances the performance.

An additional proof of this conclusion can be drawn from the Mott Schottky measurements. The charge transport of minority charge carriers through QNR is due to the diffusion while drift mechanism governs the charge transport at SCR [21]. The overall collection efficiency is governed by the electric field distribution which depends upon the built in potential  $V_{bi}$  and applied potential across the solar cell.

Fig. 7 shows the Mott Schottky plot for micro-structured and planar Si solar cells (Fig. S4). The depletion width for both the solar cell were calculated using an expression  $W = \left( \frac{2\epsilon_0\epsilon_r V_{bi}}{qN_A} \right)^{1/2}$  where,  $\epsilon_0$ ,  $\epsilon_r$ ,  $V_{bi}$  and  $N_A$  are the permittivity of vacuum, dielectric constant, built in potential, and doping density, respectively [43,44]. The built in potential ( $V_{bi}$ ) can be calculated as  $V_{bi} = \left( \frac{k_B T}{q} \right) \ln \left( \frac{N_A N_D}{n_i^2} \right)$ . The value of  $V_{bi}$  is found to be 0.63 V and 0.52 V for micro-structured and planar solar cell. The higher value of  $V_{bi}$  for micro-structured solar cell tends to increase the  $V_{OC}$  which eventually increases the efficiency of the fabricated micro-structured Si solar cells.

#### 4. Conclusions

In conclusion, we showed the record-high efficiency of 16.9% micro-scale structured Si solar cell with a large size of  $3.2 \times 3.2 \text{ cm}^2$ . We demonstrate the case where the structured Si solar cell outperforms its planar counterpart due to (1) efficient carrier collection in the pillar structures, (2) appropriate choice of pillar diameter to maximize the carrier collection versus surface area increase and (3) the reduced reflectance from the micro-structured devices. Furthermore, IS technique was employed to reveal the mechanism for higher  $V_{OC}$  in a micro-structured solar cell as compared to the planar Si solar cell. The obtained intense electric field distribution and optical enhancement in the pillar structure as compared to the planar Si signifies that we have conceived a micro-structured device to take the advantage over both the optical and electrical characteristics.

#### Acknowledgements

This research was supported by Basic Science Research Program (NRF-2015R1D1A1A01059165, NRF-2016R1D1A1A09917491, NRF-

2015H1D3A1066311) through the National Research Foundation (NRF) of Korea and Korea Institute of Energy Technology Evaluation and Planning (KETEP) by the Ministry of Trade, Industry & Energy (KETEP-20143030011960) for the New & Renewable Energy Core Technology Program. Pankaj Yadav, Malkeshkumar Patel and Hyunyub Kim equally contributed to this work.

#### Appendix A. Supplementary data

Supplementary data associated with this article can be found, in the online version, at [10.1016/j.materresbull.2017.05.027](https://doi.org/10.1016/j.materresbull.2017.05.027).

#### References

- [1] K. Seo, Y.J. Yu, P. Duane, W. Zhu, H. Park, M. Wober, et al., Si microwire solar cells: improved efficiency with a conformal SiO<sub>2</sub> layer, *ACS Nano*. 7 (2013) 5539–5545, doi:<http://dx.doi.org/10.1021/nn401776x>.
- [2] J.-Y. Jung, Z. Guo, S.-W. Jee, H.-D. Um, K.-T. Park, M.S. Hyun, et al., A waferscale Si wire solar cell using radial and bulk p-n junctions, *Nanotechnology* 21 (2010) 445303, doi:<http://dx.doi.org/10.1088/0957-4484/21/44/445303>.
- [3] M.D. Kelzenberg, D.B. Turner-Evans, M.C. Putnam, S.W. Boettcher, R.M. Briggs, J.Y. Baek, et al., High-performance Si microwire photovoltaics, *Energy Environ. Sci.* 4 (2011) 866, doi:<http://dx.doi.org/10.1039/c0ee00549e>.
- [4] E.a. Santori, N.C. Strandwitz, R.L. Grimm, B.S. Brunshwig, H.a. Atwater, N.S. Lewis, Operation of lightly doped Si microwires under high-level injection conditions, *Energy Environ. Sci.* 7 (2014) 2329, doi:<http://dx.doi.org/10.1039/c4ee00202d>.
- [5] E.a. Santori, J.R. Maiolo III, M.J. Bierman, N.C. Strandwitz, M.D. Kelzenberg, B.S. Brunshwig, et al., Photoanodic behavior of vapor-liquid-solid-grown, lightly doped, crystalline Si microwire arrays, *Energy Environ. Sci.* 5 (2012) 6867, doi:<http://dx.doi.org/10.1039/c2ee03468a>.
- [6] M. Li, Y. Li, W. Liu, L. Yue, R. Li, Y. Luo, et al., Metal-assisted chemical etching for designable monocrystalline silicon nanostructure, *Mater. Res. Bull.* 76 (2016) 436–449, doi:<http://dx.doi.org/10.1016/j.materresbull.2016.01.006>.
- [7] O. Gunawan, K. Wang, B. Fallahazad, Y. Zhang, X. Tutuc, S. Guha, High performance wire-array silicon solar cells, *Prog. Photovolt. Res. Appl.*, 19, (n.d.) 307–312, doi:[10.1002/pip.1027](https://doi.org/10.1002/pip.1027).
- [8] H. Kim, J. Kim, E. Lee, D.W. Kim, J.H. Yun, J. Yi, Effect of the short collection length in silicon microscale wire solar cells, *Appl. Phys. Lett.* 102 (2013) 193904, doi:<http://dx.doi.org/10.1063/1.4804581>.
- [9] J. Kim, E. Lee, M. Ju, H. Kim, J. Yi, S.-J. Moon, et al., Surface-concentrated light and efficient carrier collection in microhole-patterned Si solar cells, *Opt. Express* 21 (2013) A607–A615, doi:<http://dx.doi.org/10.1002/pt.2291>.
- [10] M. Gharghi, E. Fathi, B. Kante, S. Sivorthaman, X. Zhang, Heterojunction silicon solar cells, *Nano Lett.* 12 (2012) 6278–6282.
- [11] E. Lee, Y. Kim, M. Gwon, D.W. Kim, S.H. Baek, J.H. Kim, Comparative experimental and simulative investigations of radial p-n junction Si microwire array solar cells, *Sol. Energy Mater. Sol. Cells* 103 (2012) 93–97, doi:<http://dx.doi.org/10.1016/j.solmat.2012.04.023>.
- [12] K.-T. Park, Z. Guo, H.-D. Um, J.-Y. Jung, J.M. Yang, S.K. Lim, et al., Optical properties of Si microwires combined with nanoneedles for flexible thin film photovoltaics, *Opt. Express* 19 (2011) A41–A50, doi:<http://dx.doi.org/10.1364/OE.19.000A41>.
- [13] Y. Li, X.Y. Song, Y.L. Song, P.F. Ji, F.Q. Zhou, M.L. Tian, et al., Characterization of electronic structures from CdS/Si nanoheterostructure array based on silicon

- nanoporous pillar array, *Mater. Res. Bull.* 74 (2016) 507–510, doi:<http://dx.doi.org/10.1016/j.materresbull.2015.11.023>.
- [14] K. Zhou, S.-W. Jee, Z. Guo, S. Liu, J.-H. Lee, Enhanced absorptive characteristics of metal nanoparticle-coated silicon nanowires for solar cell applications, *Appl. Opt.* 50 (2011) G63–G68, doi:<http://dx.doi.org/10.1364/AO.50.000G63>.
- [15] L.-B. Luo, L.-H. Zeng, C. Xie, Y.-Q. Yu, F.-X. Liang, C.-Y. Wu, et al., Light trapping and surface plasmon enhanced high-performance NIR photodetector, *Sci. Rep.* 4 (2014) 3914, doi:<http://dx.doi.org/10.1038/srep03914>.
- [16] K.Q. Peng, X. Wang, L. Li, Y. Hu, S.T. Lee, Silicon nanowires for advanced energy conversion and storage, *Nano Today* 8 (2013) 75–97, doi:<http://dx.doi.org/10.1016/j.nantod.2012.12.009>.
- [17] C. Xie, J. Jie, B. Nie, T. Yan, Q. Li, P. Lv, et al., Schottky solar cells based on graphene nanoribbon/multiple silicon nanowires junctions, *Appl. Phys. Lett.* 100 (2012) 1–5, doi:<http://dx.doi.org/10.1063/1.4711205>.
- [18] L. Luo, C. Xie, X. Wang, Y. Yu, Surface plasmon resonance enhanced highly efficient planar silicon solar cell, *Nano Energy* 9 (2014) 112–120, doi:<http://dx.doi.org/10.1016/j.nanoen.2014.07.003>.
- [19] C.-Y. Wu, Z.-Q. Pan, Y.-Y. Wang, C.-W. Ge, Y.-Q. Yu, J.-Y. Xu, et al., Core-shell silicon nanowire array? Cu nanofilm Schottky junction for a sensitive self-powered near-infrared photodetector, *J. Mater. Chem. C* 4 (2016) 10804–10811, doi:<http://dx.doi.org/10.1039/C6TC03856E>.
- [20] P. Yadav, K. Pandey, B. Tripathi, C.M. Kumar, S.K. Srivastava, P.K. Singh, et al., An effective way to analyse the performance limiting parameters of polycrystalline silicon solar cell fabricated in the production line, *Sol. Energy* 122 (2015) 1–10, doi:<http://dx.doi.org/10.1016/j.solener.2015.08.005>.
- [21] P. Yadav, K. Pandey, B. Tripathi, M. Kumar, Investigation of interface limited charge extraction and recombination in polycrystalline silicon solar cell: using DC and AC characterization techniques, *Sol. Energy* 116 (2015) 293–302, doi:<http://dx.doi.org/10.1016/j.solener.2015.04.011>.
- [22] J. Kim, M. Kim, H. Kim, K. Song, E. Lee, D.W. Kim, et al., Effective light management of three-dimensionally patterned transparent conductive oxide layers, *Appl. Phys. Lett.* 101 (2012) 1–5, doi:<http://dx.doi.org/10.1063/1.4756940>.
- [23] P. Krogstrup, H.I. Jørgensen, M. Heiss, O. Demichel, J.V. Holm, M. Aagesen, et al., Single-nanowire solar cells beyond the Shockley–Queisser limit, *Nat. Photonics* 7 (2013) 1–5, doi:<http://dx.doi.org/10.1038/nphoton.2013.32>.
- [24] F. Priolo, T. Gregorkiewicz, M. Galli, T.F. Krauss, Silicon nanostructures for photonics and photovoltaics, *Nat. Nanotechnol.* 9 (2014) 19–32, doi:<http://dx.doi.org/10.1038/NNANO.2014.271>.
- [25] S. Jeong, M.D. McGehee, Y. Cui, All-back-contact ultra-thin silicon nanowire solar cells with 13.7% power conversion efficiency, *Nat. Commun.* 4 (2013) 2950, doi:<http://dx.doi.org/10.1038/ncomms3950>.
- [26] J. Wallentin, N. Anttu, D. Asoli, M. Huffman, I. Aberg, M.H. Magnusson, et al., InP nanowire array solar cells achieving 13.8% efficiency by exceeding the ray optics limit, *Science* 339 (2013) 1057–1060, doi:<http://dx.doi.org/10.1126/science.1230969>.
- [27] J. Gao, O.I. Lebedev, S. Turner, Y.F. Li, Y.H. Lu, Y.P. Feng, et al., Phase selection enabled formation of abrupt axial heterojunctions in branched oxide nanowires, *Nano Lett.* 12 (2011) 275–280, doi:<http://dx.doi.org/10.1021/nl2035089>.
- [28] J. Kim, J.-H. Yun, H. Kim, Y. Cho, H.-H. Park, M.M.D. Kumar, et al., Transparent conductor-embedding nanocones for selective emitters: optical and electrical improvements of Si solar cells, *Sci. Rep.* 5 (2015) 9256, doi:<http://dx.doi.org/10.1038/srep09256>.
- [29] J.-H. Yun, E. Lee, H.-H. Park, D.-W. Kim, W.a. Anderson, J. Kim, et al., Incident light adjustable solar cell by periodic nanolens architecture, *Sci. Rep.* 4 (2014) 6879, doi:<http://dx.doi.org/10.1038/srep06879>.
- [30] M.D. Kumar, H. Kim, J. Kim, Periodically patterned Si pyramids for realizing high efficient solar cells by wet etching process, *Sol. Energy* 117 (2015) 180–186, doi:<http://dx.doi.org/10.1016/j.solener.2015.04.034>.
- [31] J. Oh, H.-C. Yuan, H.M. Branz, An 18.2%-efficient black-silicon solar cell achieved through control of carrier recombination in nanostructures, *Nat. Nanotechnol.* 7 (2012) 743–748, doi:<http://dx.doi.org/10.1038/nnano.2012.166>.
- [32] J.E. Garland, D.J. Crain, J.P. Zheng, C.M. Sulyma, D. Roy, J.E. Garland, et al., Electro-analytical characterization of photovoltaic cells by combining voltammetry and impedance spectroscopy: voltage dependent parameters of a silicon solar cell under controlled illumination and temperature, *Energy Environ. Sci.* 4 (2011) 485–498, doi:<http://dx.doi.org/10.1039/c0ee00307g>.
- [33] D.J. Crain, J.E. Garland, S.E. Rock, D. Roy, Quantitative characterization of silicon solar cells in the electro-analytical approach: combined measurements of temperature and voltage dependent electrical parameters, *Anal. Methods* 4 (2012) 106, doi:<http://dx.doi.org/10.1039/c1ay05455d>.
- [34] O. Breitenstein, J. Bauer, A. Lotnyk, J. Wagner, Superlattices and Microstructures Defect induced non-ideal dark I–V characteristics of solar cells, *Superlattices Microstruct.* 45 (2009) 182–189, doi:<http://dx.doi.org/10.1016/j.spmi.2008.10.025>.
- [35] I. Mora-Seró, G. Garcia-Belmonte, P.P. Boix, M.A. Vázquez, J. Bisquert, Impedance spectroscopy characterisation of highly efficient silicon solar cells under different light illumination intensities, *Energy Environ. Sci.* 2 (2009) 678–686, doi:<http://dx.doi.org/10.1039/b812468j>.
- [36] P. Yadav, B. Tripathi, K. Pandey, M. Kumar, Solar Energy Materials & Solar Cells Investigating the charge transport kinetics in poly-crystalline silicon solar cells for low-concentration illumination by impedance spectroscopy, *Sol. Energy Mater. Sol. Cells.* 133 (2015) 105–112, doi:<http://dx.doi.org/10.1016/j.solmat.2014.10.031>.
- [37] O. Breitenstein, P. Altermatt, K. Ramspeck, A. Schenk, The origin of ideality factors  $n > 2$  of shunts and surfaces in the dark I–V curves of solar cells, 21 st Eur. Photovolt. Sol. Energy Conf. (2006) 625–628. (10.1.1.68.2414).
- [38] O. Breitenstein, J.P. Rakotoniaina, M.H. Al Rifai, M. Werner, Shunt types in crystalline silicon solar cells, *Prog. Photovoltaics Res. Appl.* 12 (2004) 529–538, doi:<http://dx.doi.org/10.1002/pip.544>.
- [39] J.E. Garland, D.J. Crain, D. Roy, Impedance spectroscopy coupled with voltammetry for quantitative evaluation of temperature and voltage dependent parameters of a silicon solar cell, *Sol. Energy* 85 (2011) 2912–2923, doi:<http://dx.doi.org/10.1016/j.solener.2011.08.029>.
- [40] H.-S. Kim, I. Mora-Sero, V. Gonzalez-Pedro, F. Fabregat-Santiago, E.J. Juarez-Perez, N.-G. Park, et al., Mechanism of carrier accumulation in perovskite thin-absorber solar cells, *Nat. Commun.* 4 (2013) 2242, doi:<http://dx.doi.org/10.1038/ncomms3242>.
- [41] I. Mora-Sero, L. Bertoluzzi, V. Gonzalez-Pedro, S. Gimenez, F. Fabregat-Santiago, K.W. Kemp, et al., Selective contacts drive charge extraction in quantum dot solids via asymmetry in carrier transfer kinetics, *Nat. Commun.* 4 (2013) 2272, doi:<http://dx.doi.org/10.1038/ncomms3272>.
- [42] V.A. Online, P. Yadav, B. Tripathi, K. Pandey, M. Kumar, Recombination kinetics in a silicon solar cell at low concentration: electro-analytical characterization of space-charge and quasi-neutral regions †, *Phys. Chem. Chem. Phys.* 16 (2014) 15469, doi:<http://dx.doi.org/10.1039/c4cp01115e>.
- [43] C.S. Solanki, *Solar Photovoltaics: Fundamentals, Technologies and Applications*, PHI Learning Pvt Ltd., 2015.
- [44] M.A. Green, Crystalline and thin-film silicon solar cells: state of the art and future potential, *Sol. Energy* 74 (2003) 181–192, doi:[http://dx.doi.org/10.1016/S0038-092X\(03\)00187-7](http://dx.doi.org/10.1016/S0038-092X(03)00187-7).